EUROPEAN ORGANIZATION FOR NUCLEAR RESEARCH

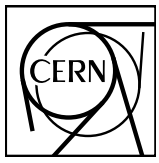

CERN-EP-2016-xxx
8 December 2016

Systematic studies of correlations between different order flow harmonics in Pb–Pb collisions at $\sqrt{s_{\rm NN}} = 2.76$ TeV

ALICE Collaboration *

Abstract

The correlations between event-by-event fluctuations of ~~amplitudes of anisotropic flow harmonics~~ anisotropic flow harmonic amplitudes have been measured in Pb–Pb collisions at $\sqrt{s_{\rm NN}} = 2.76$ TeV with the ALICE detector at the Large Hadron Collider. The results were obtained with the ~~multi-particle~~ multiparticle correlation observables dubbed ~~symmetric cumulants~~Symmetric Cumulants. These observables are robust against ~~systematic~~ biases originating from non-flow effects. The centrality dependence of ~~correlation~~ correlations between the higher order harmonics (~~v_3,~~ the quadrangular v_4 and pentagonal v_5 flow) and the lower order harmonics (the elliptic v_2 and triangular v_3 ~~)~~ flow), as well as the transverse momentum dependence of correlations ~~of~~ between v_3 and v_2 ~~,~~ and between v_4 and v_2 ~~correlations~~ are presented. The results are compared to calculations from viscous hydrodynamics and A Multi-Phase Transport (AMPT) model calculations. The ~~comparison~~ comparisons to viscous hydrodynamic ~~model demonstrates~~ models demonstrate that the different order harmonic correlations respond differently to the initial conditions ~~or~~ and the temperature dependence of the ratio of shear viscosity to ~~the entropy density ratio~~ entropy density (η/s). ~~The small~~ A small average value of η/s is favored regardless of initial conditions ~~is favored and the small η/s with the~~ and the AMPT initial condition ~~is~~ yields results closest to the measurements. Correlations between the magnitudes of v_2, v_3 and v_4 ~~magnitudes~~ show moderate $p_{\rm T}$ dependence in mid-central collisions. This might be an indication of possible viscous corrections ~~for~~ to the equilibrium distribution at hadronic freeze-out, which might help to understand the possible contribution of bulk viscosity in ~~a~~ the hadronic phase of the system. Together with ~~the~~ existing measurements of individual flow harmonics~~the presented results~~ , the results presented here provide further constraints on initial conditions and the transport properties of the system produced in heavy-ion collisions.

*See Appendix A for the list of collaboration members

1 Introduction

The main emphasis of the ultra-relativistic heavy-ion ~~collisions~~ collision programs at the Relativistic Heavy Ion Collider (RHIC) and the Large Hadron Collider (LHC) is to study the deconfined phase of ~~the~~ strongly interacting nuclear matter, the Quark-Gluon Plasma (QGP). This matter exhibits strong collective and anisotropic flow in the plane transverse to the beam direction, which is driven by ~~the~~ anisotropic pressure gradients, resulting in more particles emitted in the direction of the largest gradients. The large elliptic flow discovered at RHIC energies [**?**] ~~continues to increase also~~ is also observed at LHC energies [**? ?**]. This has been predicted by calculations utilizing viscous hydrodynamics [**? ? ? ? ? ?**]. These calculations also demonstrated that the shear viscosity to the entropy density ratio (η/s) of ~~QGP~~ the QGP in heavy-ion collisions at RHIC and LHC energies is close to a universal lower bound $1/4\pi$ [**?**]~~in heavy-ion collisions at RHIC and LHC energies~~.

The temperature dependence of ~~the~~ η/s has some generic features that most ~~of the~~ known fluids obey. For instance, one such general behavior is that ~~the~~ this ratio typically reaches its minimum value close to the phase transition region [**?**]. It was shown, using kinetic theory and quantum mechanical considerations [**?**], that $\eta/s \sim 0.1$ would be the correct order of magnitude for the lowest possible shear viscosity to entropy density ratio value found in nature. Later it was demonstrated that an exact lower bound $(\eta/s)_{\mathrm{min}} = 1/4\pi \approx 0.08$ can be calculated using ~~the~~ AdS/CFT correspondence [**?**]. Hydrodynamical simulations ~~support as well~~ also support the view that η/s of the QGP ~~matter~~ is close to that limit [**?**]. This may have important implications for other fundamental physics goals. It is argued that such a low value might imply that thermodynamic trajectories for the expanding matter would lie close to the quantum chromodynamics (QCD) critical end point, which is another subject of intensive experimental ~~quest~~study [**? ?**].

Anisotropic flow [**?**] is traditionally quantified with n^{th}-order flow coefficients v_n and corresponding symmetry plane angles Ψ_n in ~~the~~ a Fourier decomposition of the particle azimuthal distribution in the plane transverse to the beam direction [**?**]:

$$E\frac{\mathrm{d}^3N}{\mathrm{d}p^3} = \frac{1}{2\pi}\frac{\mathrm{d}^2N}{p_{\mathrm{T}}\mathrm{d}p_{\mathrm{T}}\mathrm{d}\eta}\left\{1+2\sum_{n=1}^{\infty} v_n(p_{\mathrm{T}},\eta)\cos[n(\varphi-\Psi_n)]\right\}, \tag{1}$$

where E, p, p_{T}, φ and η are the particle's energy, momentum, transverse momentum, azimuthal angle and pseudorapidity, respectively, and Ψ_n is the azimuthal angle of the symmetry plane of the n^{th}-order harmonic. Harmonic v_n can be calculated as $v_n = \langle\cos[n(\varphi-\Psi_n)]\rangle$, where the brackets denote an average over all particles in all events. The anisotropic flow in heavy-ion collisions is ~~understood as~~ typically understood as the hydrodynamic response of the produced matter to spatial deformations of the initial energy density profile [**?**]. This profile fluctuates event-by-event due to fluctuating ~~position~~ positions of the constituents inside the colliding nuclei, which implies that v_n also fluctuates [**? ?**]. The recognition of the importance of flow fluctuations led to the discovery of triangular and higher flow harmonics [**? ?**] as well as to the ~~correlation~~ correlations between different v_n harmonics [**? ?**]. The higher order harmonics are expected to be sensitive to fluctuations in the initial conditions and to the magnitude of η/s [**? ?**], while v_n correlations have the potential to discriminate between these two respective contributions [**?**].

Difficulties in extracting η/s in heavy-ion collisions can be attributed mostly to the fact that it strongly depends on the specific choice of the initial conditions in the models used for comparison [**? ? ?**]. ~~The viscous effects~~ Viscous effects also reduce the magnitude of the elliptic flow. Furthermore, the magnitude of η/s used in hydrodynamic calculations should be considered as an average over the temperature evolution of the expanding fireball as it is known that η/s ~~of other fluids~~ depends on temperature. In addition, part of the elliptic flow can also originate from the hadronic phase [**? ? ?**]. Therefore, ~~knowledge of~~ both the temperature dependence of η/s and the relative contributions from the partonic and hadronic phases should be understood better to quantify the η/s of the ~~partonic fluid~~QGP.

An important input to the hydrodynamic model simulations is the initial distribution of energy density in the transverse plane (the initial density profile), which is usually estimated from the probability distribution of nucleons in the incoming nuclei. This initial energy density profile can be quantified by calculating the distribution of the spatial ~~eccentricity~~eccentricities ε_n [**?**],

$$\varepsilon_n e^{in\Phi_n} = -\{r^n e^{in\phi}\}/\{r^n\}, \tag{2}$$

where the curly brackets denote the average over the transverse plane, i.e. ~~,~~$\{\cdots\} = \int dxdy\ e(x,y,\tau_0)$ $(\cdots)$, r is the distance to the system's center of mass, $e(x,y,\tau_0)$ is the energy density at the initial time τ_0, and Φ_n is the participant plane angle (see ~~Ref~~Refs. [**?** **?**]). There ~~are~~ is experimental and theoretical ~~evidences~~evidence [**?** **?** **?**] that the lower order harmonic coefficients, v_2 and v_3, are to a good approximation linearly proportional to the deformations in the initial energy density in the transverse plane (e.g. $v_n \propto \varepsilon_n$ for ~~n=~~n = 2 or 3). Harmonic v_4 and higher order flow coefficients can arise from initial anisotropies in the same harmonic [**?** **?** **?** **?**] (linear response) or can be induced by ~~lower-order~~ lower order harmonics [**?** **?**] (nonlinear response). ~~The~~ Therefore, the higher harmonics ($n > 3$) ~~could~~ can be understood as superpositions of linear and nonlinear responses, through which they are correlated with lower order harmonics [**?** **?** **?** **?**]. When the order of the harmonic is large, the nonlinear response contribution in viscous hydrodynamics is dominant and ~~become larger for~~ increases in more peripheral collisions [**?** **?**]. The magnitude of the viscous corrections as a function of p_{T} for v_4 and v_5 is sensitive to the ansatz used for the viscous distribution function, ~~a~~ and to the correction for the equilibrium distribution at hadronic freeze-out [**?** **?**]. Hence~~the~~ , studies of the higher order ($n > 3$) to lower order (v_2 or v_3) harmonic correlations and their p_{T} dependence can help to understand the viscous correction to the momentum distribution at hadronic freeze-out which is among the least understood ~~part~~ parts of hydrodynamic calculations ~~[? ?]~~[**?** **?** **?** **?**].

Recently, the ALICE Collaboration measured for the first time the ~~new multiparticle observables, the~~ Symmetric 2-harmonic 4-particle Cumulants (SC), new multiparticle observables which quantify the relationship between event-by-event fluctuations of two different flow harmonics [**?**]. The new observables are particularly robust against few-particle non-flow correlations and they provide independent information to recently analyzed symmetry plane correlators [**?**]. It was demonstrated that they are sensitive to the temperature dependence of η/s of the expanding medium and therefore simultaneous descriptions of ~~different order harmonic correlations~~ correlations between different order harmonics would constrain both the initial conditions and the medium properties [**?** **?**]. In this article, we have extended the analysis of SC observables to higher order Fourier harmonics (up to 5$^{\mathrm{th}}$ order) as well as to the measurement of the p_{T} dependence of correlations for the lower order harmonics (v_3-v_2 and v_4-v_2). We also include extensive ~~comparison~~ comparisons to hydrodynamic and AMPT model calculations. In Sec. 2 we summarize our findings from the previous work [**?**] and present the analysis methods. The experimental ~~setting~~ setup and measurements are described in Sec. 3 and the sources of systematic uncertainties are explained in Sec. 4. The results of the measurements are presented in Sec. 5. In Sec. 6 we present comparisons to theoretical calculations. Various theoretical models used in ~~the~~ this article are described in Sec. 6. Finally, Sec. 7 summarizes our findings.

2 Experimental Observables

~~The existing~~ Existing measurements provide an estimate of the average value of ~~QGP's~~ η/s of the QGP, both at RHIC and LHC energies. What remains uncertain is how the η/s of the QGP depends on temperature (T). The temperature dependence of η/s in the QGP was discussed in [**?**]. The effects ~~to~~ on hadron spectra and elliptic flow were studied in [**?**] for different ~~parametrizations~~ parameterizations of $\eta/s(T)$. A more systematic study with ~~the~~ event-by-event EKRT+viscous hydrodynamic calculations has ~~been just~~ just been initiated in Ref. [**?**], where the first (and only rather qualitative) possibilities ~~where~~ were investigated (see Fig. 1 therein). The emerging picture is that the study of individual flow

harmonics v_n ~~will unlikely~~ alone are unlikely to reveal the details of ~~$\eta/s(T)$ dependence~~ the temperature dependence of η/s. It was ~~demonstrated already~~ already demonstrated in [**?**] that different $\eta/s(T)$ parameterizations can lead to the same centrality dependence of individual flow harmonics. In Ref. [**?**] new flow observables were introduced which quantify the degree of correlation between two different harmonics v_m and v_n. These new observables have the potential to discriminate between the contributions to anisotropic flow development from initial conditions and from the transport properties of the QGP [**?**]. Therefore their ~~measurements would provide the experimental constrains of the~~ measurement would provide experimental constraints on theoretical predictions for the individual stages of heavy-ion system evolution independently. In addition, it turned out that correlations of different flow harmonics are sensitive to the temperature dependence of η/s [**?**], to which individual flow harmonics are weakly sensitive [**?**].

For reasons discussed in [**?** **?**], the correlations between different flow harmonics cannot be studied experimentally with the same set of observables introduced in [**?**]. Based on [**?**], ~~the~~ new flow observables obtained from multiparticle correlations, ~~so-called~~ *Symmetric Cumulants (SC)*, were introduced. SC observables are nearly insensitive to nonflow and quantify the correlation of the amplitudes of two different flow harmonics. The first measurements of SC observables were recently published by the ALICE Collaboration in [**?**].

The SC observables are defined as:

$$\begin{aligned}\langle\langle\cos(m\varphi_1+n\varphi_2-m\varphi_3-n\varphi_4)\rangle\rangle_c &= \langle\langle\cos(m\varphi_1+n\varphi_2-m\varphi_3-n\varphi_4)\rangle\rangle \\ &\quad -\langle\langle\cos[m(\varphi_1-\varphi_2)]\rangle\rangle\langle\langle\cos[n(\varphi_1-\varphi_2)]\rangle\rangle \\ &= \langle v_m^2 v_n^2\rangle - \langle v_m^2\rangle\langle v_n^2\rangle\,, \end{aligned} \tag{3}$$

with the condition $m \neq n$ for two positive integers m and n (for details see Sec. IV C in [**?**]):~~-~~

$$\begin{aligned}\langle\langle\cos(m\varphi_1+n\varphi_2-m\varphi_3-n\varphi_4)\rangle\rangle_c &= \langle\langle\cos(m\varphi_1+n\varphi_2-m\varphi_3-n\varphi_4)\rangle\rangle \\ &\quad -\langle\langle\cos[m(\varphi_1-\varphi_2)]\rangle\rangle\langle\langle\cos[n(\varphi_1-\varphi_2)]\rangle\rangle \\ &= \langle v_m^2 v_n^2\rangle - \langle v_m^2\rangle\langle v_n^2\rangle\,, \end{aligned}$$

~~with the condition $m \neq n$ for two positive integers m and n~~. In this article SC(m,n) normalized ~~with~~ by the product $\langle v_m^2\rangle\langle v_n^2\rangle$ [**?** **?**] ~~,~~is denoted by NSC(m,n):

$$\mathrm{NSC}(m,n) \equiv \frac{\mathrm{SC}(m,n)}{\langle v_m^2\rangle\langle v_n^2\rangle}\,. \tag{4}$$

Normalized symmetric cumulants reflect only the ~~degree~~ strength of the correlation which is expected to be insensitive to the magnitudes of v_m and v_n, while SC(m,n) ~~contains both the degree of the correlations between~~ has contributions from both the correlations between the two different flow harmonics and the individual v_n harmonics. In Eq. (4) the products in the denominator are obtained ~~with~~ from two-particle correlations using a pseudorapidity gap of $|\Delta\eta| > 1.0$ which suppresses biases from few-particle nonflow correlations. For the two two-particle correlations which appear in the definition of SC(m,n) in Eq. (4) the pseudorapidity gap is not needed, since nonflow is suppressed by construction in this case. This was verified by HIJING model simulations in [**?**].

The ALICE measurements [**?**] have revealed that fluctuations of v_2 and v_3 are anti-correlated, while fluctuations of v_2 and v_4 are correlated in all centralities [**?**]. However, the details of the centrality dependence differ in the fluctuation-dominated (most central) and the geometry-dominated (mid-central)

regimes [**?**]. The observed centrality dependence of SC(4,2) cannot be captured ~~with the~~ by models with constant η/s~~dependence~~, indicating clearly that the temperature dependence of η/s plays an important role. These results were also used to discriminate between different parameterizations of initial conditions. It was demonstrated that in the fluctuation-dominated regime (central collisions), MC-Glauber initial conditions with binary ~~collisions~~ collision weights are favored over wounded nucleon weights [**?**]. The first theoretical studies of SC observables can be found in Refs. [**? ? ? ? ?**].

3 Data Analysis

~~A sample of~~ Data recorded by ALICE in Pb–Pb collisions at $\sqrt{s_{\rm NN}} = 2.76$ TeV ~~recorded by ALICE~~ during the 2010 heavy-ion run at the LHC is used for this analysis. Detailed descriptions of the ALICE detector can be found in [**? ? ?**]. The Time Projection Chamber (TPC) was used to reconstruct charged particle tracks and measure their momenta with full azimuthal coverage in the pseudorapidity range $|\eta| < 0.8$. Two scintillator arrays (V0) which cover the pseudo-rapidity ranges $-3.7 < \eta < -1.7$ and $2.8 < \eta < 5.1$ were used for triggering and the determination of centrality [**?**]. The trigger conditions and the event selection criteria are identical to those described in [**? ?**]. Approximately 10^7 minimum-bias Pb–Pb events with a reconstructed primary vertex within ± 10 cm from the nominal interaction point ~~in~~ along the beam direction are selected. ~~Charged~~ Only charged particles reconstructed in the TPC in $|\eta| < 0.8$ and $0.2 < p_{\rm T} < 5$ GeV/c were ~~selected~~taken for the analysis. The charged track quality cuts described in [**?**] were applied to minimize contamination from secondary charged particles and fake tracks. The track reconstruction efficiency and contamination ~~of charged particles~~ were estimated from HIJING Monte Carlo simulations [**?**] combined with a GEANT3 [**?**] detector model and were found to be independent of the collision centrality. The reconstruction efficiency increases from 70% to 80% for particles with $0.2 < p_{\rm T} < 1$ GeV/c and remains constant at $(80 \pm 5)\%$ for $p_{\rm T} > 1$ GeV/c. The estimated contamination by secondary charged particles from weak decays and photon conversions is less than 6% at $p_{\rm T} = 0.2$ GeV/c and falls below 1% for $p_{\rm T} > 1$ GeV/c. The $p_{\rm T}$ cut-off of 0.2 GeV/c reduces event-by-event biases due to small reconstruction efficiency at lower $p_{\rm T}$, while the high $p_{\rm T}$ cut-off of 5 GeV/c reduces the ~~contribution to the anisotropies from jets~~ effects of jets on the measured correlations. Reconstructed TPC tracks were required to have at least 70 space points (out of a maximum of 159). Only tracks with a transverse distance of closest approach (DCA) to the primary vertex less than 3 mm, both in the longitudinal and transverse ~~direction~~directions, are accepted. This reduces the contamination from secondary tracks produced in the detector material, particles from weak decays, etc. Tracks with kinks (~~the~~ i.e. tracks that appear to change direction due to multiple scattering ~~,~~ or $K^{\pm}$ decays) were rejected.

4 Systematic Uncertainties

The systematic uncertainties are estimated by varying the event and track selection criteria. All systematic checks described here are performed independently. ~~All results of~~ The SC(m,n) ~~with a selected criterion~~ values resulting from each variation are compared to ones from the default event and track selection described in the previous section~~. The differences between the default results and the ones obtained from the variation of the selection criteria~~ , and differences are taken as ~~systematic uncertainty of~~ the systematic uncertainty due to each individual source. The contributions from different sources were added in quadrature to obtain the total systematic uncertainty.

The event centrality was determined by the V0 detectors [**?**] with better than 2% resolution for the whole centrality range analyzed. The systematic uncertainty from the centrality determination was evaluated by using the TPC and Silicon Pixel Detector (SPD) [**?**] detectors instead of the V0 detectors. The systematic uncertainty from the centrality ~~determinations~~ determination is about 3% both for SC(5,2) and SC(4,3), and 8% for SC(5,3).

As described in Sec. 3, the reconstructed vertex position along the beam axis (z-vertex) is required to be

located within 10 cm of the interaction point (IP) to ensure ~~a~~ uniform detector acceptance for ~~the~~ tracks within $|\eta| < 0.8$~~for all the vertices~~. The systematic uncertainty from the z-vertex cut was estimated by reducing the z-vertex ~~to 8cm~~ range to 8 cm and was found to be less than 3%.

The analyzed events were recorded with two settings of the ~~L3~~ magnet polarity and the resulting data sets have almost ~~the same number~~ equal numbers of events. Events with both magnet ~~polarity were used for~~ polarities were used in the default analysis, and the systematic uncertainties were evaluated from the variation between each of the two magnetic field settings. ~~Moreover, the effects from~~ The uncertainty on the p_{T} ~~dependence reconstruction efficiency were taken into systematic uncertainty~~dependent track reconstruction efficiency was also taken into account. Magnetic polarity variation and reconstruction efficiency effects ~~are~~ contribute less than 2% to the systematic uncertainty.

The systematic uncertainty due to the track reconstruction was estimated from ~~comparison~~ comparisons between results for the so-called standalone TPC tracks with the same parameters as described in Sec. 3, and tracks from a combination of the TPC and the Inner Tracking System (ITS) detectors with tighter selection criteria. To correct for non-uniform azimuthal acceptance due to dead zones in the SPD, and to get the best transverse momentum resolution, approach of hybrid selection with SPD hit and/or ITS refit tracks combined with TPC were used. Then each track reconstruction strategy was evaluated by varying the threshold on parameters used to select the tracks at the reconstruction level. The systematic difference of up to 12% was observed in SC(m,n) from the different track selections. In addition, we applied the like-sign technique to estimate non-flow ~~contribution in~~ contributions to SC(m,n). The difference between results obtained by selecting all charged particles and results obtained after either selecting only positively or only negatively charged particles was the largest contribution to the systematic uncertainty and it is about 7% for SC(4,3) and 20% for SC(5,3).

Another large contribution to the systematic uncertainty originates from ~~the non-uniform reconstruction efficiencyin azimuthal angle~~azimuthal non-uniformities in the efficiency. In order to estimate its effects, we use the AMPT model (see Sec. 6) which ~~have flat uniform distribution of azimuthal angles~~has a uniform distribution in azimuthal angle. Detector inefficiencies ~~was~~ were introduced to mimic the non-uniform azimuthal distribution in the data. For the observables SC(5,2), SC(5,3) and SC(4,3) the variation due to non-uniform acceptance is about 9%, 17% and 11%, respectively. Overall, the systematic uncertainties are larger for ~~the~~ SC(5,3) and SC(5,2) than for the lower harmonics of SC(m,n). This is because v_n ~~are decreasing with n increasing and become~~ decreases with increasing n and becomes more sensitive to azimuthal modulation due to detector imperfections.

5 Results

The centrality dependence of the higher order harmonic correlations (SC(4,3), SC(5,2) and SC(5,3)) are presented in Fig. 1 and compared to the lower order harmonic correlations (SC(4,2) and SC(3,2)) which ~~are taken from~~ were measured in [**?**]. The correlation between v_3 and v_4 is negative, and similarly for v_3 and v_2, while the other correlations are all positive, which reveals that v_2 and v_5 ~~,~~ as well as v_3 and v_5 are correlated ~~as~~ like v_2 and v_4, while v_3 and v_4 are anti-correlated ~~as~~ like v_3 and v_2.

The higher order flow harmonic correlations (SC(4,3), SC(5,2) and SC(5,3)) are much smaller compared to the lower order harmonic correlations~~(SC(3,2) and SC(4,2))~~. In particular SC(5,2) is 10 times smaller than SC(4,2) and SC(4,3) is about 20 times smaller ~~that~~ than SC(3,2).

However, unlike SC(m,n), the NSC(m,n) results with the higher order flow harmonics show almost the same order of the correlation strength as the lower order flow harmonic correlations (NSC(3,2) or NSC(4,2)). The NSC(4,3) magnitude is comparable to NSC(3,2) and one finds that a hierarchy, NSC(5,3) $>$ NSC(4,2) $>$ NSC(5,2), holds for centrality ranges ~~$> 20\% >$~~ 20% within the errors ~~shown on the panel (b)~~ as shown in Fig. 1b. These results indicate that the lower order harmonic correlations ~~(SC(3,2) and~~

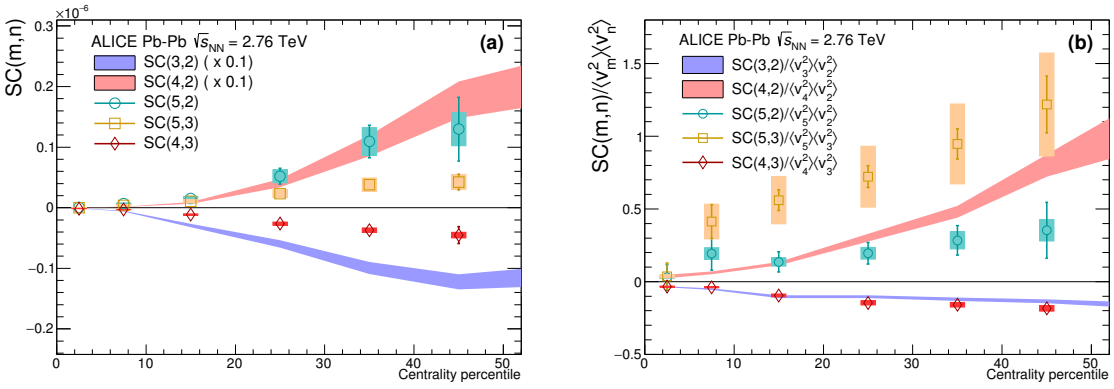

Fig. 1: SC(m,n) (a) and NSC(m,n) (b) with flow ~~harmonic~~ harmonics up to 5$^{\text{th}}$ order in Pb–Pb collisions at $\sqrt{s_{\text{NN}}}$ = 2.76 TeV. The lower order harmonic correlations (SC(3,2), SC(4,2), NSC(3,2) and NSC(4,2)) are taken from [**?**] and shown as bands. Note that the systematic and statistical errors are combined ~~quadratically~~ in quadrature for these lower order harmonic correlations and SC(4,2) and SC(3,2) ~~on the panel (a)~~ are scaled by a factor of 0.1. Systematical errors are represented with boxes.

~~SC(4,2))~~ are larger than higher order harmonic correlations~~(SC(4, 3), SC(5, 2) and SC(5,3)),~~ not only because of the correlation strength itself but also because of the strength of the individual flow harmonics. SC(5,2) is stronger than SC(5,3), but ~~as for NSC,~~ the normalized correlation between v_5 and v_3 is stronger than the normalized correlation between v_5 and v_2.

It can be seen ~~on the panel (a)~~ in Fig. 1a that the lower order harmonic correlations ~~(SC(3,2) and SC(4,2)) and SC(~~as well as SC(5,2) increase non-linearly ~~toward~~ towards peripheral collisions. In the case of SC(5,3) and SC(4,3), the centrality dependence is weaker than for the other harmonic correlations and a monotonic increase is observed~~for these harmonic correlations~~. NSC(5,3) shows the strongest normalized correlation among all harmonics ~~and NSC(4,2), NSC(~~while NSC(5,2) shows ~~a weak~~ the weakest centrality dependence. Both NSC(3,2) and NSC(4,3) show a monotonic increase toward peripheral collisions with the similar magnitude.

To study the p_{T} dependence of SC(m,n), we ~~change~~ systematically vary the low p_{T} cut-off, instead of using independent p_{T} ~~interval~~intervals, in order to avoid large statistical fluctuations in the results. Various minimum p_{T} cuts from 0.2 to 1.5 GeV/c are applied. The ~~results of~~ p_{T} ~~dependence of~~ dependent results for SC(3,2) and SC(4,2) with minimum p_{T} cuts ~~,~~ $0.2 < p_{\text{T}} < 0.7$ GeV/c ~~, are shown on the panel (a)~~ are shown in Fig. 2a. The strength of SC(m,n) becomes larger as the minimum p_{T} increases. ~~This~~ These p_{T} dependent correlations have much stronger centrality dependence, ~~where~~ with SC(m,n) ~~gets~~ getting much larger as the centrality or the minimum p_{T} cut increase. NSC(3,2) and NSC(4,2) with different minimum cuts are shown ~~on the panel (b) and (d) in Fig~~in Figs. 2b and 2d. The strong p_{T} dependence observed in SC(m,n) is not seen in NSC(m,n). The NSC(m,n) results are ~~aligned all together and consistent in~~ consistent within the errors for all minimum p_{T} cuts. This indicates that the p_{T} dependence of SC(m,n) is dominated by the p_{T} dependence of the $\langle v_n \rangle$ values. The minimum p_{T} cuts are extended from 0.8 to 1.5 GeV/c and the results are shown ~~on the panel (c) and (d) in Fig~~in Figs. 2c and 2d. While SC(m,n) ~~show the~~ shows similar trends as for $p_{\text{T}} < 0.8$ GeV/c, NSC(m,n) tends to decrease with increasing p_{T}~~or the centrality~~. The p_{T} dependence ~~for~~ of NSC(3,2) is not clearly seen and it is consistent with no p_{T} dependence within the ~~current~~ statistical and systematic errors for the centrality range $< 30\%$~~and shows~~ , while showing a moderate decreasing trend ~~for~~ with increasing p_{T} for the $> 30\%$ centrality range. NSC(4,2) shows a moderate decreasing trend as p_{T} ~~or the centrality increase~~increases. These observations are strikingly different from p_{T} dependence of the individual flow harmonics, where the relative flow fluctuations $\sigma_{v_2}/\langle v_2 \rangle$ [**?**] are independent of transverse momentum

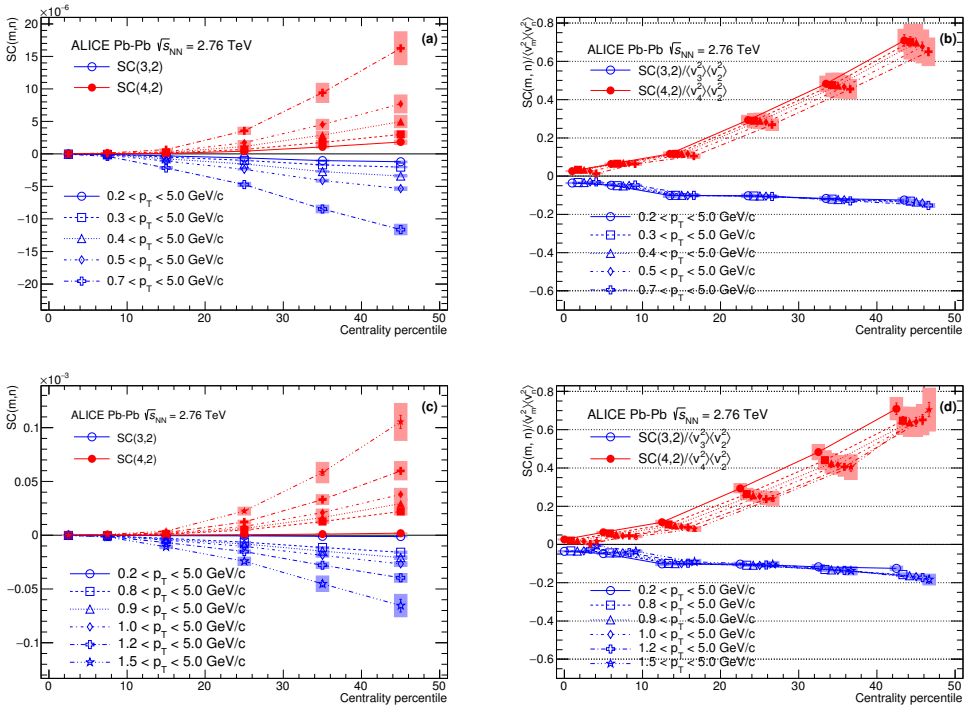

Fig. 2: SC(3,2) and SC(4,2) with ~~various minimum p_T cuts~~ low ((~~(~~a) and high (c) ~~)~~ minimum p_T cuts, and ~~results of~~ normalized SC(3,2) and SC(4,2) ((b) and (d)) in Pb–Pb collisions at $\sqrt{s_{NN}} = 2.76$ TeV. ~~The panel~~ Panels (a) and (b) show the results for the minimum p_T range ~~,~~$0.2 < p_T < 0.7$ GeV/c and ~~the panel~~ panels (c) and (d) are for the minimum p_T range ~~,~~$0.8 < p_T < 1.5$ GeV/c. Note that NSC data points from each minimum p_T in a centrality percentile bin are shifted for visibility.

up to $p_{\mathrm{T}} \sim 8$ GeV/c (see Fig. 3 in Ref. [**?**]).

6 Model Comparisons

We have compared the centrality dependence of our observables with ~~the~~ event-by-event EKRT+viscous hydrodynamic calculations [**?**], where the initial energy density profiles are calculated using a next-to-leading order perturbative-QCD+saturation model [**?** **?**]. The subsequent spacetime evolution is described by relativistic dissipative fluid dynamics with different parameterizations for the temperature dependence of the shear viscosity to entropy density ratio $\eta/s(T)$. This model gives a good description of the charged hadron multiplicity and the low p_{T} region of the charged hadron spectra at RHIC and the LHC (see ~~Fig~~Figs. 11-13 in [**?**]). Each of the $\eta/s(T)$ parameterizations is adjusted to reproduce the measured v_n from central to mid-peripheral collisions (see Fig. ~~14~~ 15 in [**?**]).

The VISH2+1 [**?** **?**] event-by-event calculations for relativistic heavy-ion collisions are based on (2+1)-dimensional viscous hydrodynamics which describes both the QGP phase and the highly dissipative and even off-equilibrium late hadronic stage with fluid dynamics. With ~~well tuned transport coefficients , decoupling temperature~~well-tuned transport coefficients and decoupling temperature, and given initial condition discussed later, it ~~could~~ can describe the p_{T} spectra and different flow harmonics at RHIC and the LHC [**?** **?** **?** **?**]. Three different initial conditions (MC-Glauber, MC-KLN and AMPT) along with different constant η/s values are used in the model [**?**]. Traditionally, the Glauber model constructs the initial entropy density ~~from contributions of~~ with contributions from the wounded nucleon and binary collision density profiles [**?**], and the KLN model assumes that the initial entropy density is proportional to the initial gluon density calculated from the corresponding ~~k_T~~ k_{T} factorization formula [**?**]. In the Monte Carlo versions (MC-Glauber and MC-KLN) [**?** **?** **?**], additional initial state fluctuations are introduced through ~~the position fluctuation~~ position fluctuations of individual nucleons inside the colliding nuclei. For the AMPT initial conditions [**?** **?** **?**], the fluctuating energy density profiles are constructed from the energy decompositions of individual partons, which fluctuate in both momentum and position coordinate. Compared with the MC-Glauber and MC-KLN initial conditions, the additional Gaussian smearing in the AMPT initial conditions gives rise to non-vanishing initial local flow velocities [**?**].

The centrality dependence of the SC observables is compared to that in the AMPT model [**?** **?** **?**]. Even though thermalization could be achieved in collisions of very large nuclei and/or at extremely high energy [**?**], the dense matter created in heavy-ion collisions may not reach full thermal or chemical equilibrium as a result of its finite volume and short ~~time scale~~lifetime. To address such non-equilibrium many-body dynamics, AMPT has been developed, which includes both initial partonic and final hadronic interactions and the transition between these two phases of matter. For the initial conditions, the AMPT model uses the spatial and momentum distributions of hard minijet partons and soft strings from the HIJING model [**?** **?**]. The AMPT model can be run in two main configurations, the default and the string melting model [1]. In the default version, partons are recombined with their parent strings when they stop interacting. The resulting strings are later converted into hadrons using the Lund string fragmentation model [**?** **?**]. In the string melting version, the initial strings are melted into partons whose interactions are described by the ZPC parton cascade model [**?**]. These partons are then combined into the final state hadrons via a quark coalescence model. In both configurations, the dynamics of the subsequent hadronic matter is described by a hadronic cascade based on A Relativistic Transport (ART) model [**?**] which also includes resonance decays. The third version used in this article is based on the string melting configuration ~~,~~ in which the hadronic rescattering phase is switched off to study its influence ~~to~~ on the development of anisotropic flow. Even though the string melting version of AMPT [**?** **?**] reasonably reproduces particle yields, p_{T} spectra, and v_2 of ~~low~~-low p_{T} pions and kaons in central and mid-central Au–Au collisions at $\sqrt{s_{\mathrm{NN}}} = 200$ GeV and Pb–Pb collisions at $\sqrt{s_{\mathrm{NN}}} = 2.76$ TeV [**?**], it

[1] The input parameters used in both configurations are: $\alpha_s = 0.33$, a partonic cross-section of 1.5 mb, while the Lund string fragmentation parameters were set to $\alpha = 0.5$ and $b = 0.9$ GeV^{-2}.

was seen clearly in ~~the~~ a recent study [**?**] that it fails to quantitatively reproduce the ~~harmonic~~ flow coefficients of identified hadrons (v_2, v_3, v_4 and v_5) at $\sqrt{s_{\rm NN}} = 2.76$ TeV. It turns out that the radial flow in AMPT is 25% lower than ~~the measured value~~ that measured at the LHC, which ~~indicates that the unrealistically low radial flow in AMPT~~ is responsible for the quantitative disagreement [**?**]. The details of ~~configurations of AMPT settings used for~~ the AMPT configurations used in this article and the comparisons of $p_{\rm T}$~~differential~~ differential v_n for pions, kaons and protons to the data can be found in [**?**].

6.1 Low Order Harmonic Correlations

SC(3,2) and SC(4,2) are compared to several theoretical calculations. The event-by-event EKRT+viscous hydrodynamic predictions with the different parameterizations for the temperature dependence of the shear viscosity to entropy density ratio $\eta/s(T)$ are shown in Fig. 2 of Ref. [**?**]. ~~It has been~~ In this previous work it was demonstrated that NSC(3,2) ~~observable~~ is sensitive mainly to the initial conditions, while NSC(4,2) ~~observable~~ is sensitive to both the initial conditions and the system properties, which is consistent with the predictions from [**?**]. However, the sign of NSC(3,2) is ~~positive in the models in 0-10~~negative in the data in 0–10% central collisions while it is ~~negative in data. In the most central collisions~~ positive in the models where the anisotropies originate mainly from fluctuations~~, i. e. the initial ellipsoidal geometry characteristic for mid-central collisions plays little role in this regime.~~ . This observation helps ~~to understand better~~ us to better understand the fluctuations in initial energy density. NSC(4,2) observable shows better sensitivity for different $\eta/s(T)$ parameterizations but the model cannot describe ~~neither~~ either the centrality dependence ~~nor~~ or the absolute values. This observed ~~distinct~~ discrepancy between data and theoretical predictions indicates that the current understanding of initial conditions used to model the initial stages of heavy-ion ~~collision need~~ collisions needs to be revisited to further constrain ~~the~~ $\eta/s(T)$~~, considering the difficulties in separating the role of the η/s from the initial conditions to the final state particle anisotropies [**?** **?**]~~. The use of SC(m,n) and NSC(m,n) can provide new constraints ~~on~~ for the detailed modeling of fluctuating initial conditions. The better constraints on the initial state conditions will certainly reduce the uncertainties ~~of~~ in determining $\eta/s(T)$.

The ~~results with the comparison to~~ comparison to the VISH2+1 calculation [**?**] ~~are~~ is shown in Fig. 3. All calculations with large η/s regardless of the initial conditions ($\eta/s = 0.2$ for MC-KLN and MC-Glauber initial conditions and $\eta/s = 0.16$ for AMPT initial ~~condition~~conditions) fail to capture the centrality dependence of SC(3,2) and SC(4,2). Among the calculations with small η/s ($\eta/s = 0.08$), the one with the AMPT initial condition describes the data better both for SC(3,2) and SC(4,2) ~~in general~~ but it cannot describe the data quantitively for most of the centrality ranges. ~~Similarly~~ Similar to the event-by-event EKRT+viscous hydrodynamic calculations [**?**], the sign of the normalized NSC(3,2) in the model calculations in Fig. 3 is opposite to that in data in ~~0-10~~0–10% central collisions. NSC(3,2) does not show sensitivity to the initial conditions nor to the different η/s parameterizations used in the models and cannot be described quantitatively by these models~~quantitively. However~~. However, NSC(4,2) is sensitive both to the initial conditions and the η/s parameterizations used in the models. Even though NSC(4,2) favors both AMPT initial ~~condition~~ conditions with $\eta/s = 0.08$ and MC-Glauber initial ~~condition~~ conditions with $\eta/s = 0.20$, SC(4,2) can ~~be only described by~~ only be described by models with smaller η/s~~from AMPT and MC-Glauber initial conditions. Hence these calculations~~ . Hence the calculation with large $\eta/s = 0.20$ ~~are~~ is ruled out. We conclude that η/s should be small and ~~AMPT initial condition is~~ that AMPT initial conditions are favored by the data.

~~The~~ SC(m,n) calculated from AMPT simulations are compared ~~to~~ with data in Fig. 4. ~~As for~~ For SC(3,2), ~~none of the calculations can describe the data and the~~ the calculation with the default AMPT ~~setting follows the trend of the data closest~~settings is closest to the data, but none of the AMPT configurations can describe the data fully. The same default calculation can describe the sign and magnitude of NSC(3,2) while the hydrodynamic calculations ~~failed~~ fail to describe either of them in the most central collisions. Interestingly, the string melting AMPT ~~model~~ configuration cannot reproduce the data~~and~~

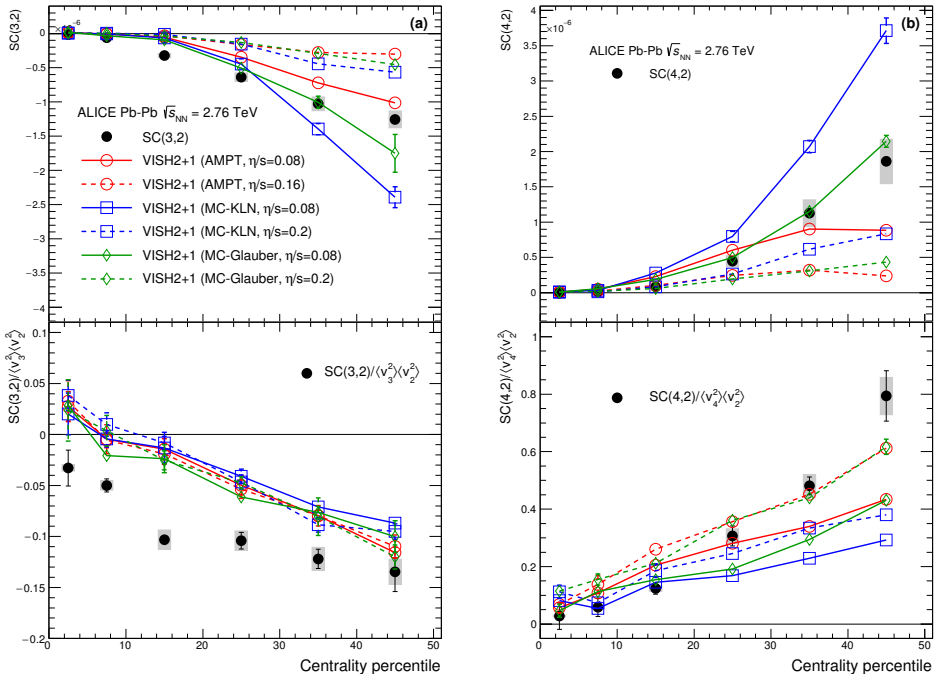

Fig. 3: SC(3,2) (a) and SC(4,2) (b) in Pb–Pb collisions at $\sqrt{s_{\rm NN}} = 2.76$ TeV are compared to various VISH2+1 calculations [**?**] with different settings. Upper (lower) panels show SC(m,n) (NSC(m,n)). Calculations with ~~three initial conditions from~~ AMPT, MC-KLN, and MC-Glauber initial conditions are drawn as different colors and markers. The η/s parameters are shown in different line styles, the small $\eta/s = 0.08$ are shown as solid lines, and large ~~$\eta/s = 0.2$~~ η/s (0.2 for MC-KLN and MC-Glauber, 0.16 for AMPT) are drawn as dashed lines.

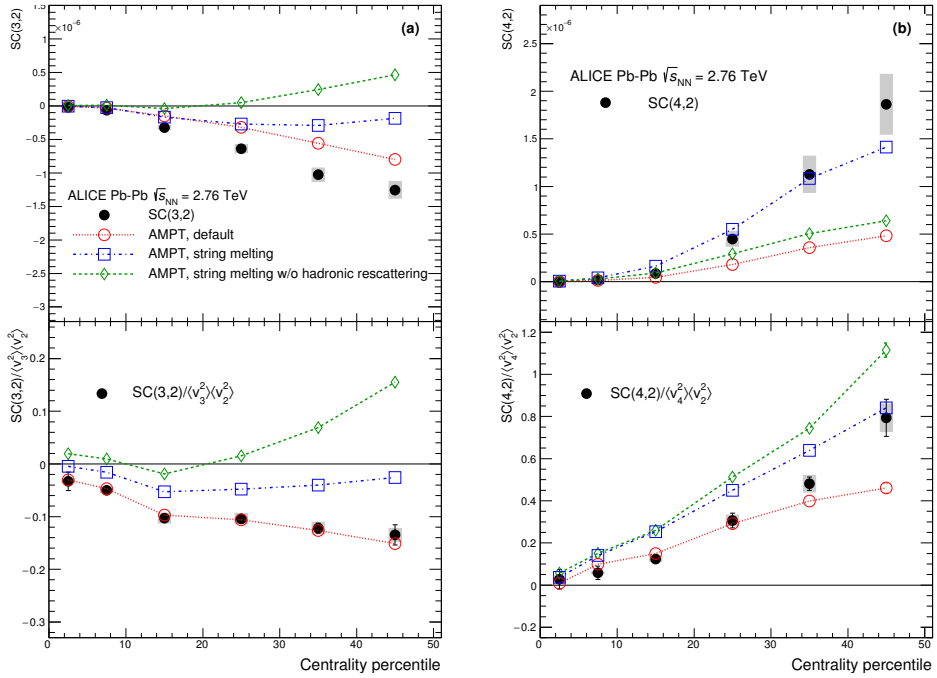

Fig. 4: SC(3,2) (a) and SC(4,2) (b) in Pb–Pb collisions at $\sqrt{s_{\rm NN}} = 2.76$ TeV are compared to various AMPT models. Upper ~~panels~~ (lower) ~~are the results of~~ panels show SC(m,n) (NSC(m,n)).

~~the strength of the correlation is~~ , and the resulting correlations are weaker than in data. The third version based on the string melting configuration without the hadronic rescattering phase is also shown. The hadronic rescattering stage makes both SC(3,2) and NSC(3,2) stronger in the string melting AMPT model but not enough to describe the data. Further ~~we investigated~~ investigations proved why the default AMPT model can describe NSC(3,2) fairly well but underestimates SC(3,2). By taking the differences in the individual flow harmonics (v_2 and v_3) between the model and data into account, ~~we were able~~ it was possible to recover the difference in SC(3,2) between the data and the model. The discrepancy in SC(3,2) can be explained by the overestimated individual v_n values as reported in [**?**] in all the centrality ranges.

In the case of SC(4,2), the string melting AMPT model can ~~fairly well~~ describe the data fairly well while the default model underestimates it. NSC(4,2) is slightly overestimated by the ~~same~~ string melting setting which can describe SC(4,2) but the default AMPT ~~model~~ configuration can describe the data better. The influence of the hadronic rescattering phase ~~for~~ on NSC(4,2) is opposite to other observables (SC(3,2), NSC(3,2) and SC(4,2)). The hadronic rescattering makes NSC(4,2) slightly smaller. It should be noted that the ~~better agreement for~~ agreement with SC(m,n) should not be overemphasized since there are discrepancies in the individual v_n between the AMPT models and the data as ~~it~~ was demonstrated for SC(3,2). Hence the simultaneous description of SC(m,n) and NSC(m,n) should give better constraints ~~to~~ on the parameters in AMPT models.

6.2 Higher Order Harmonic Correlations

The higher order harmonic correlations (SC(4,3), SC(5,2) and SC(5,3)) are compared to several theoretical model calculations. The event-by-event EKRT+viscous hydrodynamic predictions with the different parameterizations for the temperature dependence of the shear viscosity to entropy density ratio $\eta/s(T)$ are shown in Fig. 5. **[Waiting for $\eta/s(T)$ hydro calculations from Harri Niemi et. al [?], figure will be replaced late**
While we discussed the comparison to these hydrodynamic model calculations with various temperature dependent η/s parameterizations, only two calculations with the parameters which describe the lower order harmonic correlations best are compared to the results of higher order harmonic correlations. As it can be seen in Fig. 1 from Ref. [**?**], for "param1" parameterization the phase transition from hadronic to QGP phase occurs at lowest temperature, already around 150 MeV. This parameterization is also characterized with moderate slope of $\eta/s(T)$ of decreasing (increasing) in hadronic (QGP) phase. The model calculations with the parameters for which the temperature of phase transition is larger than for "param1" can be ruled out already with the previous measurement [**?**]. As shown in Fig. 5, only the correlations between v_5 and v_2 are well described for all available centralities. On the other hand, for correlations between v_5 and v_3 the description fails in the transition towards more peripheral collisions, providing further independent constraints for the models. In the case of the correlation between v_4 and v_3, the same models underestimate the data significantly. Most notably, this measurement is so far the most dramatic example of a failure of constant η/s to describe the data.

The higher order harmonic correlations ~~(SC(4,3), SC(5,2) and SC(5,3))~~ are compared to VISH2+1 calculations [**?**], shown in Fig. 6. All the models with large η/s ~~regardless of the initial conditions~~ ($\eta/s = 0.2$ for MC-KLN and MC-Glauber, and $\eta/s = 0.16$ for AMPT initial conditions) ~~failed~~ regardless of the initial conditions fail to capture the centrality dependence of SC(5,2), SC(5,2) and SC(5,3), ~~more clearly than~~ with larger disagreements than observed for the lower order harmonic correlations~~(SC(3,2) and SC(4,2))~~. Among the models with small η/s ($\eta/s = 0.08$), the one ~~from~~ with the AMPT initial ~~condition~~ conditions describes the data much better than the ones with other initial conditions. A quite clear separation between different initial conditions is observed for these higher order harmonic correlations compared to the lower order harmonic correlations. NSC(5,2) and SC(5,3) are quite sensitive to both the initial conditions and the η/s parameterizations. ~~Similarly as the above mentioned hydrodynamic calculations~~ Similar to the hydrodynamic calculations mentioned above [**?**], the sign of ~~the~~ NSC(4,3) in these models is opposite to its ~~signature~~ sign in the data in ~~0-10~~0–10% central collisions. NSC(4,3)

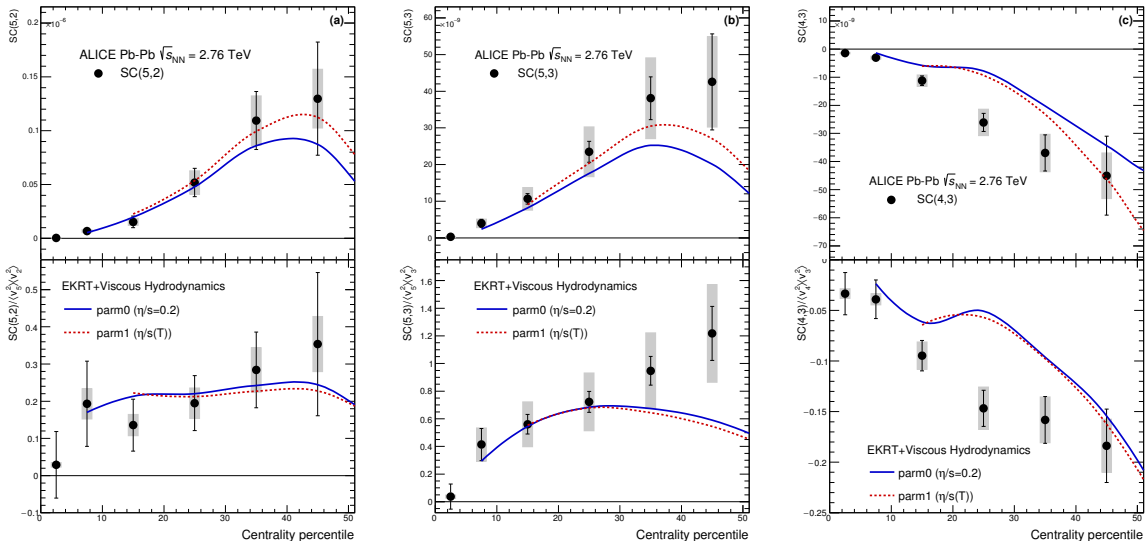

Fig. 5: ~~Results~~ Measurements of SC(5,2) (a), SC(5,3) (b) and SC(4,3) (c) in Pb–Pb collisions at $\sqrt{s_{\mathrm{NN}}} = 2.76$ TeV are compared to the event-by-event EKRT+viscous hydrodynamic calculations [**?**]. The ~~dashed~~ lines are hydrodynamic predictions with ~~various~~ two different $\eta/s(T)$ parameterizations, labeled in the same way as in [**?**]. ~~These~~ ~~SC~~Upper (~~3,2~~lower) ~~and~~ panels show SC(m,n) (~~4,2~~NSC(m,n))~~will be replaced with new figures for higher order correlations once we have the calculations from Harri Niemi et~~.al ~~[?].~~

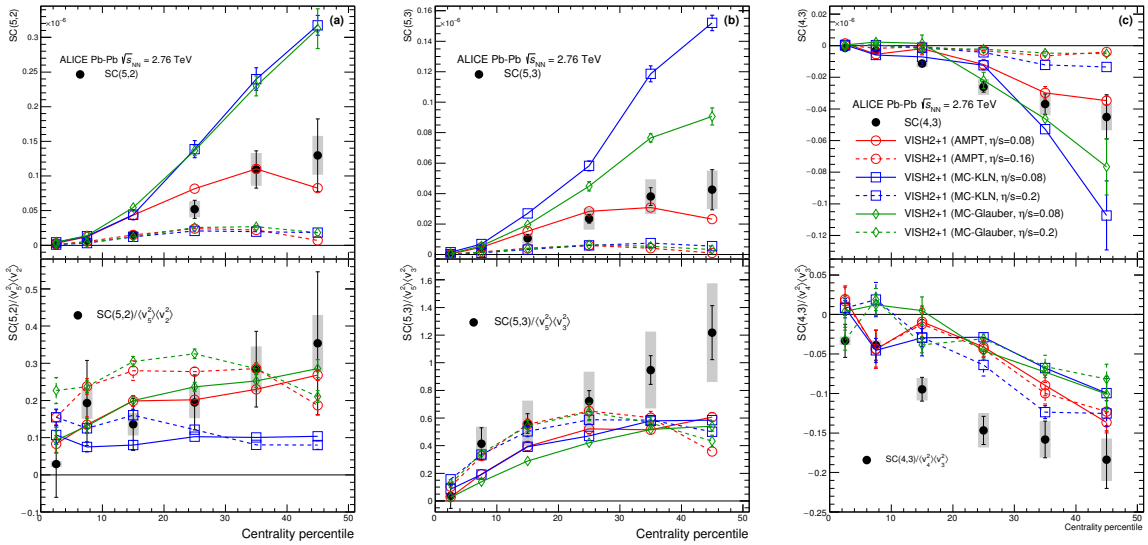

Fig. 6: Results of SC(5,2), SC(5,3) and SC(4,3) in Pb–Pb collisions at $\sqrt{s_{\mathrm{NN}}} = 2.76$ TeV are compared to various VISH2+1 calculations [**?**]. Three initial conditions from AMPT, MC-KLN and MC-Glauber are drawn as different colors and markers. The η/s parameters are shown as different line styles, the small shear viscosity ($\eta/s = 0.08$) are shown as solid lines, and large shear viscosities ($\eta/s = 0.2$ for MC-KLN and MC-Glauber, 0.16 for AMPT) are drawn as dashed lines. Upper (lower) panels ~~are the results of~~ show SC(m,n) ~~and lower panels are the results of~~ (NSC(m,n)).

shows sensitivity to both initial conditions and η/s parameterizations. The SC(4,3) ~~data is~~ results are clearly favored by smaller η/s values but NSC(4,3) cannot be described by these models quantitively.

The ~~extracted results for final state particles~~ results from AMPT simulations ~~in the same way as for the~~

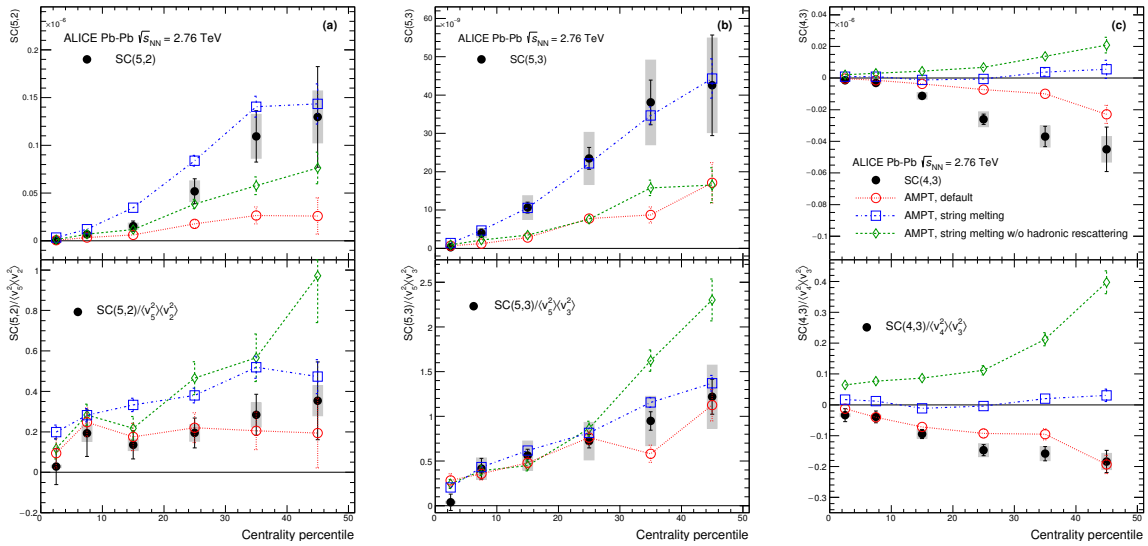

Fig. 7: Results of SC(5,2), SC(5,3) and SC(4,3) in Pb–Pb collisions at $\sqrt{s_{\rm NN}} = 2.76$ TeV are compared to various AMPT models. Upper (lower) panels ~~are the results of~~ show SC(m,n) ~~and the lower panels are the results of~~ (NSC(m,n)).

~~data are compared~~ are compared to the data in Fig. 7. The string melting AMPT model describes SC(5,3) and NSC(5,3) well. ~~The~~ However, the same setting overestimates SC(5,2) and NSC(5,2). ~~However the~~ The default AMPT model can describe NSC(5,3) and NSC(5,2) fairly well as ~~it is the case for NSC(3,2) and NSC(4,2)~~ in the case of the lower harmonics seen in Fig. 4. In the case of SC(4,3), neither of the settings can describe the data but the default AMPT model ~~follows the data closest~~ comes the closest to the data. The string melting AMPT model fails to describe SC(4,3) and NSC(4,3). In summary, the default AMPT model describes well the normalized symmetric cumulants (NSC(m,n)) from lower to higher order harmonic correlations while the string melting AMPT model overestimates NSC(5,2) and ~~underestimates (or predicts~~ predicts a very weak correlation ~~)~~ in NSC(4,3).

As discussed in Sec. 5, a hierarchy NSC(5,3) $>$ NSC(4,2) $>$ NSC(5,2) holds for centrality ranges $> 20\%$ within the errors and NSC(5,2) is smaller than NSC(5,3) while SC(5,2) is larger that SC(5,3). Except for ~~0-10~~0–10% centrality range, we found that the same hierarchy also holds ~~for~~ in the hydrodynamic calculations and the AMPT models explored in this article. The observed ~~difference between~~ reversal of the hierarchy SC(5,2) ~~and SC(5,3) (SC(5,2)~~ $>$ SC(5,3)~~)~~, can be explained by the ~~difference~~ magnitudes of the individual flow harmonics ($v_2 > v_3$). The opposite trend ~~are~~ is observed for the normalized SC (NSC(5,3) $>$ NSC(5,2)). This can be attributed to the fact that ~~the flow fluctuation is~~ flow fluctuations are stronger for v_3 than v_2 [**?**]. ~~It~~ This was claimed in Ref. [**?**] and ~~seen also~~ also seen in Ref. [**?**] based on a AMPT model. NSC(m,n) correlators increase with ~~the~~ larger η/s in hydrodynamic calculations in the 0-30% centrality range in the same way as the event plane correlations [**?** **?**]. In semi-peripheral collisions (>40%), the opposite trend is observed.

We list here the important findings from the model ~~comparison~~comparisons:

(i) ~~NSC(3,2) observable is sensitive mainly to the initial conditions, while NSC(4,2) observable is sensitive to both the initial conditions and the temperature dependence of η/s.~~

(ii) All the VISH2+1 model calculations with large η/s ~~regardless of the initial conditions failed~~ fail to capture the centrality dependence of ~~correlations~~the correlations regardless of the initial conditions.

(iii) Among the VISH2+1 model calculations with small η/s ($\eta/s = 0.08$), the one with the AMPT

initial ~~condition~~ conditions describes the data ~~better in general~~ qualitatively but it cannot describe the data quantitively for most of the centrality ranges.

(iv) The ~~correlation strength of~~ NSC(3,2) observable is sensitive mainly to the initial conditions, while the other observables are sensitive to both the initial conditions and the temperature dependence of η/s.

(v) The correlation strength between v_3 and v_2 ~~,~~and between v_4 and v_3 (NSC(3,2) and NSC(4,3)) is significantly underestimated in hydrodynamic model calculations.

(vi) The sign of NSC(3,2) in ~~0–10~~0–10% central collisions was found to be different ~~between~~ in the data and the hydrodynamic model calculations while the default AMPT model can reproduce the sign.

(vii) The default AMPT model can describe the normalized symmetric cumulants (NSC(m,n)) quantitively for most ~~of~~ centralities while the string melting AMPT model fails to describe them.

(viii) A hierarchy NSC(5,3) $>$ NSC(4,2) $>$ NSC(5,2) holds for centrality ranges $>20\%$ within the errors. This hierarchy is ~~well reproduced~~ reproduced well both by hydrodynamic and AMPT model calculations.

6.3 Transverse Momentum Dependence of Correlations between v_2, v_3 and v_4

It can be seen in Fig. 2 that for the ~~p_{T} dependence for~~ NSC(3,2) ~~is not clearly seen and it is consistent with~~ observable no p_{T} dependence ~~for~~ is seen in the centrality range $<30\%$~~and shows~~, and a moderate decreasing trend ~~for~~ with increasing p_{T} ~~for~~ is seen for the $>30\%$ centrality range. NSC(4,2) shows a moderate decreasing trend as p_{T} or the centrality increase. In ~~oder~~ order to see the trend more clearly, we show NSC(m,n) results as a function of minimum p_{T} cut in Fig. 8 ~~.~~ and Fig. 9.

NSC(3,2) and NSC(4,2) as a function of different minimum p_{T} ~~cut~~ cuts are compared to the AMPT simulations in Fig. 8 ~~. These~~ and Fig. 9, respectively. The observed p_{T} dependence for NSC(3,2) and NSC(4,2) in mid-central collisions is ~~seen also~~ also seen in AMPT simulations for higher minimum p_{T} cuts. ~~The other AMPT configurations except for the default AMPT model give~~ With the exception of the default configuration, the other AMPT settings predict a very strong p_{T} dependence above 1 GeV/c and cannot describe the magnitude of the data ~~both for~~ for both NSC(3,2) and NSC(4,2) simultaneously. In the case of NSC(3,2), the default AMPT model describes the magnitude and p_{T} dependence well in all collision centralities except for $40-50\%$ where the model underestimates the data and ~~have~~ shows a stronger p_{T} dependence than the data. As for NSC(4,2), the same model which describes NSC(3,2) ~~also can~~ can also reproduce the data well ~~expect for~~ except for the $10-20\%$ and $40-50\%$ centralities where some deviations from the data ~~both for the magnitude and p_{T} dependence~~ are observed. When the string melting AMPT model is compared to the same model with the hadronic rescattering off, it is observed that the very strong p_{T} dependence as well as the correlation strength ~~gets weaker~~ are weakened by the hadronic rescattering. This might imply that ~~the hadronic interaction is~~ hadronic interactions are the source of this observed p_{T} dependence even though the relative contributions from the partonic and hadronic ~~stage~~ stages in the final state particle distributions should be studied further.

The event-by-event EKRT+viscous hydrodynamic calculations are compared to the data in Fig. 8. In case of NSC(3,2), the hydrodynamic calculations underestimate the data as discussed in Sec 6.1 and show very weak p_{T} dependence for all centralities. The p_{T} dependence of NSC(3,2) is well described by the model calculations in all collision centralities except for 40–50% where the data shows stronger p_{T} dependence than the models. The difference between the model calculations with two different parameterizations is very small. As for NSC(4,2), the model calculations overestimate the magnitude in the 5–20% centralities and underestimate in the centrality range $>20\%$. However the p_{T} dependence is well described by the model calculations in all centralities. While the difference of the model calculations

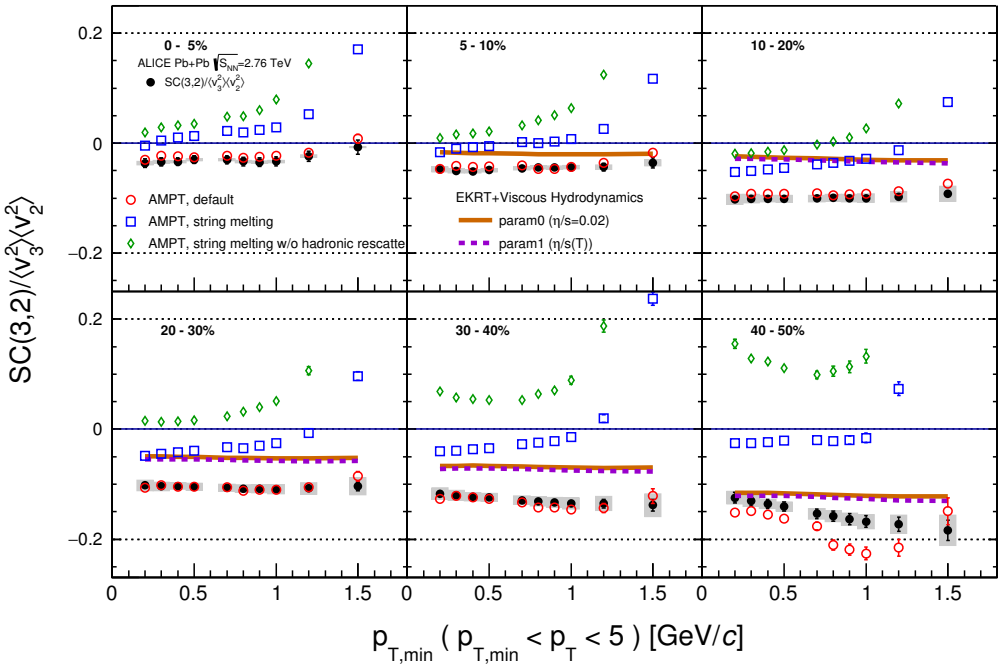

Fig. 8: NSC(3,2) ~~(Top) and NSC(4,2) (Bottom)~~ as a function of the minimum p_{T} cuts in Pb–Pb collisions at $\sqrt{s_{\mathrm{NN}}} = 2.76$ TeV are compared to various AMPT ~~models~~configurations and event-by-event EKRT+viscous hydrodynamic calculations [**?**].

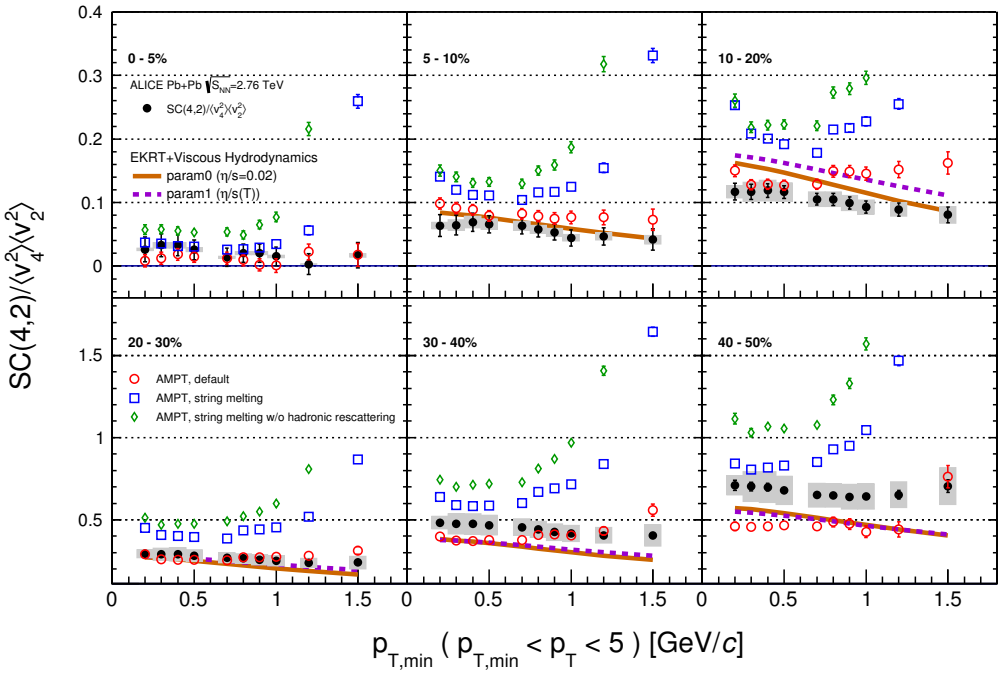

Fig. 9: NSC(4,2) as a function of the minimum p_{T} cuts in Pb–Pb collisions at $\sqrt{s_{\mathrm{NN}}} = 2.76$ TeV are compared to various AMPT configurations and event-by-event EKRT+viscous hydrodynamic calculations [**?**].

between two parameterizations in most centralities is rather small, a clear separation between two parameterizations are observed in 10–20% where both the magnitude and p_{T} dependence are different.

This observed moderate p_{T} dependence in mid-central collisions both for NSC(3,2) and NSC(4,2) might be an indication of possible viscous corrections ~~for~~ to the equilibrium distribution at hadronic freeze-out as predicted in ~~[?]~~[?]. The comparisons to hydrodynamic models can further help to understand the viscous ~~correction~~ corrections to the momentum ~~distribution~~ distributions at hadronic freeze-out ~~[? ?]~~[? ? ? ? ?].

7 Summary

In this article, we report the centrality dependence of correlation between the higher order harmonics (~~v_3,~~ v_4, v_5) and the lower order harmonics (v_2, v_3) as well as the transverse momentum dependence of the correlations between v_3 ~~-~~and v_2 and between v_4 ~~-~~and v_2~~correlations~~. The results are obtained ~~by the~~ with Symmetric 2-harmonic 4-particle Cumulants (SC). It was demonstrated earlier in [?] that this method is insensitive to the non-flow effects and free from symmetry plane correlations. We have found that fluctuations of ~~v_3-v_2 and v_4-v_3~~ SC(3,2) and SC(4,3) are anti-correlated in all centralities while fluctuations of ~~v_4-v_2,v_5-v_2 and v_5-v_3~~ SC(4,2), SC(5,2) and SC(5,3) are correlated for all centralities. ~~This measurement~~ These measurements were compared to various hydrodynamic model calculations with different initial conditions as well as different parameterizations of the temperature dependence of η/s. It is found that the different order harmonic correlations have different sensitivities to the initial conditions and the system properties. Therefore they have discriminating power in separating the effects of η/s from the initial conditions ~~to~~ on the final state particle anisotropies. The sign of ~~v_3-v_2 correlation in 0-10~~SC(3,2) in 0–10% central collisions was found to be different between the data and hydrodynamic model calculations. In the most central collisions the anisotropies originate mainly from fluctuations, where the initial ellipsoidal geometry which ~~is dominating~~ dominates in mid-central collisions plays little role. This observation might help to understand the details of the fluctuations in ~~initial conditions~~the initial stage. The comparisons to VISH2+1 ~~calculation~~ calculations show that all the models with large η/s, regardless of the initial conditions~~failed~~, fail to capture the centrality dependence of higher order correlations~~, more clearly than lower order harmonic correlations~~. Based on the tested model parameters, the ~~η/s should be small and AMPT initial condition is favored by the data~~data favors small η/s and the AMPT initial conditions. A quite clear separation of the correlation strength ~~between~~ for different initial conditions is observed for these higher order harmonic correlations compared to the lower order harmonic correlations. The default configuration of the AMPT model describes well the normalized symmetric cumulants (NSC(m,n)) for most ~~of~~ centralities and for most combinations of harmonics which were considered. Together with the measurements of individual harmonics these results provide further constraints on the system properties and help ~~discriminating~~ discriminate between theoretical models. Finally, we have found that v_3 and v_2 ~~,~~as well as v_4 and v_2 correlations have moderate p_{T} dependence in mid-central collisions. This might be an indication of possible viscous corrections ~~for~~ to the equilibrium distribution at hadronic freeze-out. The results presented in this article can be used to further optimize model parameters and put better constraints on the initial conditions and the transport properties of nuclear matter in ultra-relativistic heavy-ion collisions.

Acknowledgements

A The ALICE Collaboration